Catalysis Science & Technology

ROYAL SOCIETY OF CHEMISTRY

PAPER

View Article Online
View Journal | View Issue

Cite this: *Catal. Sci. Technol.*, 2022, 12, 5274

The influence of solvent composition on the coordination environment of the Co/Mn/Br based *para*-xylene oxidation catalyst as revealed by EPR and ESEEM spectroscopy†‡

Rebekah L. Taylor, *[a] Duncan Housley, [b] Michael Barter, [c] Adrian Porch, [c] Keith Whiston, [b] Andrea Folli *[a] and Damien M. Murphy [a]

The industrially important *para*-xylene oxidation reaction, based on a Co/Mn/Br catalyst, operates in a water/acetic acid (H_2O/AcOH) solvent system. The correct H_2O/AcOH ratio of the solvent is crucial in controlling the reaction yields and selectivities. However, the influence of this variable solvent system on the catalyst structure and coordination environment is not well understood. Using UV-vis spectroscopy, we observed the formation of tetrahedral Co^{2+} species when the solvent composition was below 10 wt% H_2O. These were considered to be tetrahedral Co^{2+} species with either 2 or 3 coordinating Br^- ligands. The pronounced CW EPR linewidth changes observed in the Mn^{2+} signals revealed a strong correlation on the solvent H_2O content. Detailed analysis revealed that these variations in the linewidth were attributed to the changing coordination sphere around the Mn^{2+} centres, with a maximum linewidth occurring at 8–10 wt% H_2O. The narrow linewidths below 8 wt% H_2O were found to result from substitution of H_2O/AcOH ligands by Br, whereas above 8 wt% H_2O a further narrowing of the linewidth was actually caused by greater amounts of H_2O coordination. To confirm this, 3-pulse ESEEM measurements on the Mn^{2+} were conducted in the solvent compositions corresponding to 3, 8, 13.7 and 20 wt% H_2O. The results showed a marked change in the number (n) of coordinated H_2O molecules (ranging from n = 0, 0, 1.0 to 4.0 respectively for the 3–20 wt% H_2O content). For the first time, these findings provide a crucial insight into the relationship between solvent composition and catalyst structure in this industrially important catalytic reaction.

Received 15th March 2022,
Accepted 19th May 2022

DOI: 10.1039/d2cy00496h

rsc.li/catalysis

Introduction

Terephthalic acid (hereafter abbreviated as PTA) is a very important and valuable commodity chemical used most notably in the production of polyethylene terephthalate (commonly known as PET) *via* co-polymerisation with ethylene glycol (Scheme 1). PET is used widely in consumer applications, from food and drinks packaging to the manufacture of fibres in clothing and upholstery. The production of PTA *via* aerobic catalytic autoxidation of *para*-xylene using a Co/Mn/Br based catalyst in acetic acid (AcOH)/water mixtures at *ca.* 200 °C and 15 bar, is one of the world's largest industrial-scale chemical processes, with over 60 existing plants worldwide producing upwards of 75 Mt *per annum* of PTA.[1] Despite the extremely well-refined process chemistry and success of this industrial process, surprisingly there remains considerable uncertainty surrounding key aspects of the catalytic mechanism, including the structure of the actual catalyst under operating conditions.

In the commercial PTA process the catalyst, which is initially introduced as $Co(OAc)_2$, $Mn(OAc)_2$ and HBr in acetic acid solution, experiences a solvent composition in which the water concentration is continuously controlled within the reactor. The precise nature of the Co/Mn/Br catalyst, including hydration conditions of the Co and Mn centres in solution, is exceedingly difficult to characterise, mostly due to the high temperatures and pressures in combination with the very acidic conditions. Furthermore, it has also been proposed that dimers, trimers, or higher oligomers of these solvated and potentially bridged metal ions could also coexist in solution.[2,3] Elucidation of the catalyst structure is of paramount importance, since catalytic activity and solvent

[a] *School of Chemistry, Cardiff University, Main Building, Park Place, Cardiff, CF10 3AT, UK. E-mail: TaylorRL3@cardiff.ac.uk, follia@cardiff.ac.uk*
[b] *The Wilton Centre, Koch Technology Solutions Ltd., Wilton, Redcar, TS10 4RE, UK*
[c] *School of Engineering, Cardiff University, The Parade, Cardiff CF24 3AA, UK*

† Electronic supplementary information (ESI) available. See DOI: https://doi.org/10.1039/d2cy00496h

‡ Dataset available from Cardiff University, https://doi.org/10.17035/d.2022.0198346445

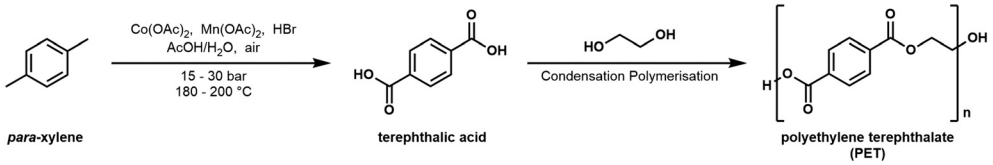

Scheme 1 Oxidation of *para*-xylene to terephthalic acid (PTA) and subsequent co-polymerisation to polyethylene terephthalate (PET).

composition are inherently linked.[4] Solvent composition is known to be one of the most important parameters influencing catalytic activity. Changes in $[H_2O]/[AcOH]/[AcO^-]$ ratios can affect the coordination environment of the Co/Mn/Br catalyst,[2,3,5] with consumption of acetic acid being also influenced by changes in pressure and temperature.[6] High water concentration leads to decreased reaction rates and increased acetic acid consumption, whereas low water concentration within the reactor also results in increased acetic acid consumption to CO and CO_2.[6,7] A good compromise seems to be achieved by operating between 5 and 15 wt% of water in solution;[6] however, such experimental evidence has yet to find a deeper fundamental understanding of the catalyst structure under variable solvent conditions.

Owing to the paramagnetic nature of the Mn^{2+} and Co^{2+} centres in the catalyst, electron paramagnetic resonance (EPR) spectroscopy, here used in combination with UV-vis spectroscopy, offers an ideal characterisation technique to study the influence of the solvent composition (*i.e.*, H_2O/AcOH ratios at given Br^- concentrations) on the resulting catalyst structure. Furthermore, electron spin echo envelope modulation (ESEEM) spectroscopy is also used to identify the specific water coordination number around the Mn^{2+} centres, to understand the interaction between the metal ions and water across the industrially relevant solvent composition range. As the solvent composition is known to directly influence catalytic performance, yields and product selectivity, this work represents an important step towards removing some of the existing empiricism still present around the solvent–catalyst structure relationship in the industrial manufacture of PTA.

Results and discussion

Metal centre coordination environment

The CW EPR spectra of the $Co(OAc)_2$ (17.75 mM), $Mn(OAc)_2$ (17.75 mM) and NaBr (35.5 mM), hereafter referred to as 1/1/2 Co/Mn/Br, recorded at 363 K and at different water/acetic acid ratios are reported in Fig. 1a. The composition and

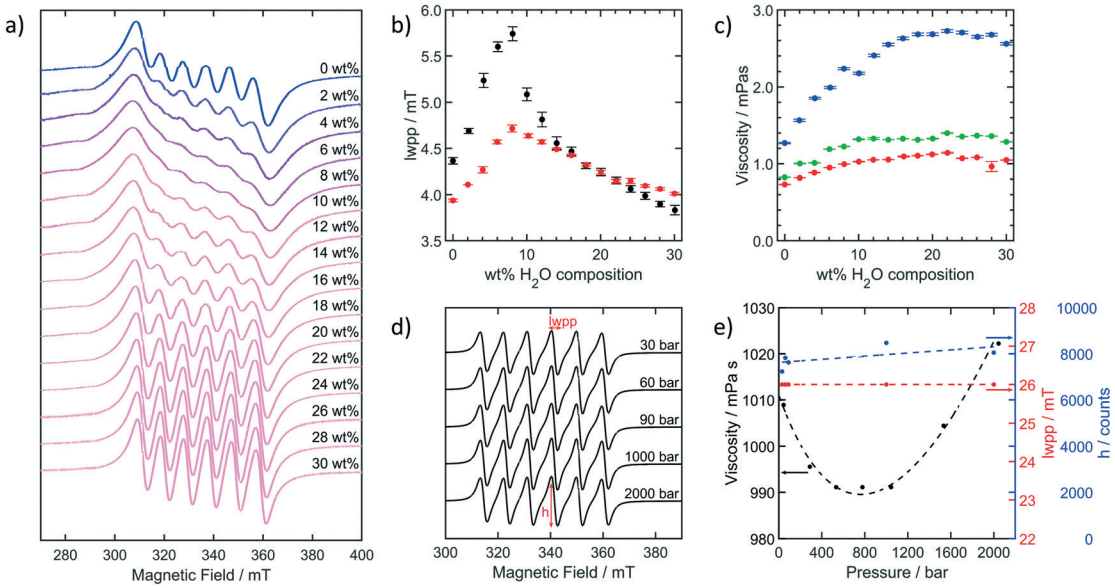

Fig. 1 a) CW X-band EPR spectra recorded at 363 K of the 1/1/2 Co/Mn/Br catalyst dissolved in varying H_2O/AcOH compositions (containing 0–30 wt% H_2O), noting the pronounced changes in linewidth for the Mn^{2+} centre as a function of different H_2O concentrations; b) changes to the peak-to-peak linewidths (lwpp) of the EPR resonance lines associated with the m_I = +1/2 transitions (justification for this choice discussed further in the ESI†) in the m_S = ±1/2 electron spin manifold of Mn^{2+} as a function of H_2O/AcOH compositions (0–30 wt% H_2O) at 296 K (red) and 363 K (black); c) changes in H_2O/AcOH solution viscosity as a function of increasing wt% H_2O at 293 K (blue), 323 K (green) and 343 K (red); d) room temperature X-band CW EPR spectra of $Mn(H_2O)_6^{2+}$ in H_2O recorded at varying solvent pressures showing no spectral variations; e) EPR linewidth (red) and signal amplitude (blue) measured from the data presented in Fig. 1d plotted as a function of pressure and the corresponding reported H_2O viscosity (black).[12]

temperature were chosen to mimic the reaction conditions, although with slow kinetics. The observed EPR spectra are indicative of a typical Mn^{2+} spin system characterised by the spin Hamiltonian parameters $S = 5/2$, $g_{eff} \approx 2.05$ and $A_{iso} \approx 260$ MHz. With varying solvent composition ranging from 0 to 30 wt% H_2O in the H_2O/AcOH system, no changes in g or A could be detected. However, a notable change in the peak-to-peak linewidth (lwpp) of the spectra was observed (Fig. 1a and b). Owing to the variety of physical and chemical parameters embedded in EPR spectral linewidths and the phenomena associated with these linewidth changes,[8,9] we have analysed the EPR linewidths as a probe for the physical chemical alterations of the (paramagnetic) catalytic species in solution as the water content increases. In particular, two different regimes can be distinguished; notably, a low water content regime (<8–10 wt% water in the solvent system) where a broadening of the EPR linewidth occurs as the water content increases, and a high water content regime (>13.7 wt% water in the solvent system) where a narrowing of the EPR linewidth occurs as the water content increases. The broadest linewidth occurs at *ca.* 8–10 wt% water in the solvent system. The observed trend measured at 363 K was also reproduced at room temperature (see ESI†).

Temperature, viscosity, concentration and coordination dynamics were considered in order to understand the physical chemical changes of the Mn^{2+} species in solution that EPR reveals. Temperature-dependent broadening or narrowing (*i.e.*, faster or slower temperature-induced relaxation) can be immediately discounted, since the temperature was carefully controlled at 363.0 ± 0.2 K across the entire study. It should also be noted that temperature variations of at least ±2.0 K are necessary to produce any observable changes in linewidth (see ESI†). Concentration broadening/narrowing due to the experimental method was also discounted, as concentration changes were outside the range of observable concentration broadening for these samples (see ESI†).

Line shape changes due to different rotational diffusion rates of the Mn^{2+} species in solution, caused for example by changes in solvent viscosity as the water content increases, can also be excluded. Viscosity measurements of the sampled solutions across the entire composition range examined in this study are reported in Fig. 1c. The trend observed in these viscosity measurements appears completely unrelated to the trend observed in the EPR linewidth measurements (Fig. 1a and b). In particular, the maximum viscosity observed at *ca.* 20 wt% H_2O in the H_2O/AcOH system does not follow the maximum broadening observed in the EPR spectra, which was detected at *ca.* 8–10 wt% H_2O. In fact, between 8–10 and 20 wt% H_2O, a narrowing of the EPR linewidth was actually observed despite the increased viscosity of the solution; this appears completely counterintuitive and cannot explain the EPR line shape variation on the basis of rotational diffusion within the Stokes–Einstein–Debye limit (*i.e.*, higher viscosity would imply broader linewidths due to reduced tumbling rates).

Furthermore, Bloembergen and Morgan have shown that the rotational averaging of Mn^{2+} species in solution does not significantly contribute to the relaxation rates of these species,[10,11] which typically would be expected to influence the linewidth. To confirm this, we conducted EPR measurements on a reference $Mn(H_2O)_6^{2+}$ species in H_2O at varying pressures, from atmospheric to 2000 bar (Fig. 1d). The results clearly show that despite a significant change in solvent viscosity upon increasing pressure (Fig. 1e),[12] no variation in EPR linewidths occurs across the same range of pressure, thus corroborating our observations that rotational averaging is not the origin of the change in EPR lineshape (Fig. 1a and b). Therefore, having excluded solvent temperature, concentration and viscosity as possible contributors to the EPR linewidth variation (Fig. 1a and b), it appears that a dynamic and changing coordination sphere surrounding the Mn^{2+} centres must instead be responsible for the subtle changes to the zero field splitting (ZFS) which in turn dictates the overall relaxation rates and therefore the EPR linewidth.[10,11] In the case of the Mn^{2+} centre in this studied system, the changes in H_2O composition are likely to result in changes to the inner coordination sphere of the Mn^{2+} centre affecting the ZFS. Therefore, it seems entirely reasonable to ascribe the observed variation in EPR linewidth to the different coordination environments of Mn^{2+}, caused by changes in solvent (H_2O) composition.

Further insights into the coordination environment of the catalyst, and the interaction of Br^- ions with metal centres, can be obtained by UV-vis spectroscopy on the Co^{2+} component of the Co/Mn/Br catalyst. This UV-vis data then provides complimentary information on the catalyst coordination obtained by CW EPR on the Mn^{2+} component, given that an analogous EPR investigation between RT > T > 363 K cannot be meaningfully performed on the Co^{2+} component of the catalyst. The high spin d^7 Co^{2+} experiences rapid spin–lattice relaxation times, caused by ZFS values typically approaching 300 GHz,[13–18] so that only frozen solution measurements are possible (below 70 K to observe a resolved CW EPR signal). By comparison, no UV-vis spectroscopy can be performed on the Mn^{2+} component (electronic transitions in the high spin d^5 centre are both spin and Laporte forbidden). Hence, EPR provides information on the Mn^{2+} component whilst UV-vis only provides information on the Co^{2+} component of the catalyst.

The UV-vis spectra for samples prepared at 17.75 mM Co^{2+} concentration in varying H_2O/AcOH ratios are shown in Fig. 2a. Upon increasing the H_2O concentration, the colour of the solution changes from a deep blue, through to purple, until a pale pink colouration is observed at *ca.* 10 wt% H_2O and above. Across all the range of H_2O/AcOH solvent compositions investigated here (from 0–20 wt% H_2O), a broad band attributed to $Co(OAc)_2$ can be observed at *ca.* 525 nm. At high H_2O compositions, a shift of this band to 519 nm can be observed, along with a corresponding decrease in the extinction coefficient. This observation is consistent with the formation of cationic $Co(OAc)^+$,[19,20] likely caused by a

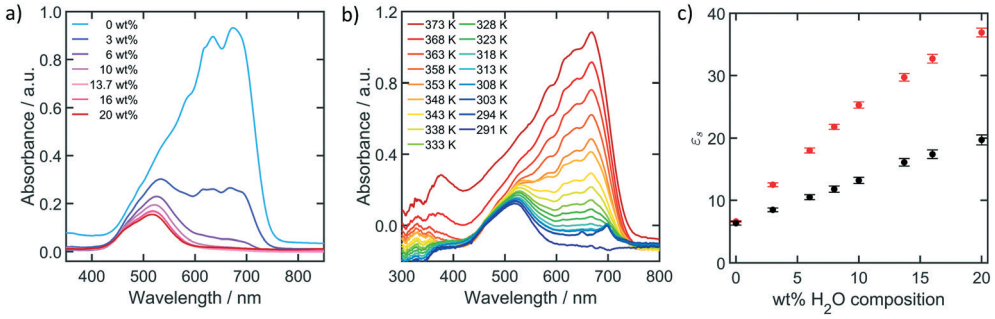

Fig. 2 UV-vis spectra of the 1/1/2 Co/Mn/Br catalyst; a) catalyst prepared using varying H_2O/AcOH ratios (from 0–20 wt%) at 298 K, and b) variable temperature spectra of the catalyst prepared using a fixed 10 wt% H_2O composition; c) the static dielectric constant ε_s of varying H_2O/AcOH ratios (from 0–20 wt%) at 298 K (red) and 363 K (black).

statistical substitution of AcO^- by H_2O at the Co^{2+} centre. As the H_2O composition is decreased below 10 wt%, a second distinct band emerges between 600–700 nm which can be assigned to a tetrahedral Co^{2+} species. *In situ* measurements reported by Partenheimer *et al.*, identified a similar species,[21] which they attributed to a tetrahedral Co^{2+} centre with 2 coordinating Br^- ligands. However additional absorption peaks are also visible at 618 and 691 nm, suggesting the presence of an equilibrium mixture of tetrahedral Co^{2+} with 2 and 3 coordinating Br^- ligands.[22]

Variable temperature UV-vis measurements using a fixed 10 wt% H_2O composition were additionally recorded (Fig. 2b). These experiments revealed that an increase in the temperature also induced the further ligation of Br^- to the Co^{2+} centre. As evident in Fig. 2b, the higher wavelength bands (between 600–700 nm) attributed to the 2 and 3 Br-coordinated tetrahedral species appear as the temperature increases. In this case, the increased Br^- coordination is consistent with the reduced dielectric properties of the solvent, promoted either by the reduced H_2O concentration or the increased temperature. This observation was confirmed by static dielectric constant measurements, as shown in Fig. 2c. The data show that both at RT and 363 K (Fig. 2c), the lower the water content in the solvent system, the lower the static dielectric constant, with ε_s reaching the value expected for glacial acetic acid when no water is present in the solvent.[23,24] In addition, the higher the temperature, the lower the static dielectric constant, with variation between the values of ε_s measured at RT and 363 K which increase as the water content is increased. Further discussion on the complex permittivity and conductivity of these samples is included in the ESI.†

Coordination of the Mn^{2+} centres (a water counting experiment)

Overall, the above combination of CW EPR and UV-vis spectroscopies has revealed that changes in H_2O content in the solvent system resulted in direct changes to the coordination environments of the Mn^{2+} and Co^{2+} centres. This is predominantly associated with Br species being removed as the water content in the system is increased. Nevertheless, questions still remain as to why the CW EPR linewidth profile shows a maximum at about 8 wt% followed by linewidth narrowing as the water content in the solvent is further increased. To better understand the role and coordination of H_2O to the Mn^{2+} centres, we performed a series of three-pulse ESEEM measurements to probe the number of H_2O molecules bonded to Mn^{2+} using a "water counting" method proposed by Hoogstraten and Britt.[25] For these measurements, the Co component of the Co/Mn/Br catalyst was removed to ensure a clear interpretation of the results (as the Mn^{2+} and Co^{2+} resonances are superimposed, see ESI†). Fig. 3a–c shows an example of the water counting data set for a reference $Mn(H_2O)_6^{2+}$ centre at the chosen magnetic induction of 349.8 mT. Fig. 3a shows the unprocessed ^1H decoupled ESEEM time profiles in H_2O and D_2O as well as the D_2O/H_2O ratio. As expected, coupling of the electron spin system to the solvent ^2H nuclei give rise to strong modulations with a period of about 440 ns; *i.e.*, the Larmor precession period for the ^2H nucleus. On the contrary, when the experiment is conducted in H_2O, no modulation was observed indicating the complete suppression of ^1H by choosing a τ in the three-pulse sequence that is a multiple integer of the ^1H Larmor precession period (a value of τ = 200 ns was used). These time profiles are indicative of both inner and outer sphere H_2O molecules. Fig. 3b reports the same set of ESEEM data for the reference $MnDTPA^{2+}$ complex (where DTPA is diethylenetriaminepentaacetic acid). In this case, the modulation is exclusively representative of outer sphere solvent molecules, as the DTPA ligand fully chelates the Mn^{2+} ion, impeding solvent molecules from directly coordinating to the metal ion. Finally, Fig. 3c reports the ratio of the D_2O/H_2O data from Fig. 3a and b. The modulation in this final time trace is thus representative of inner sphere ^2H ESEEM exclusively. The same procedure was repeated for the 1/1 Mn/Br system at four different solvent compositions including 3 wt%, 8 wt%, 13.7 wt% and 20 wt% of water. Fig. 3d–f show the resulting ESEEM time profiles following the ratioing procedure described above and superimposed to the scaled (1 to 6 D_2O molecules) time traces obtained for the

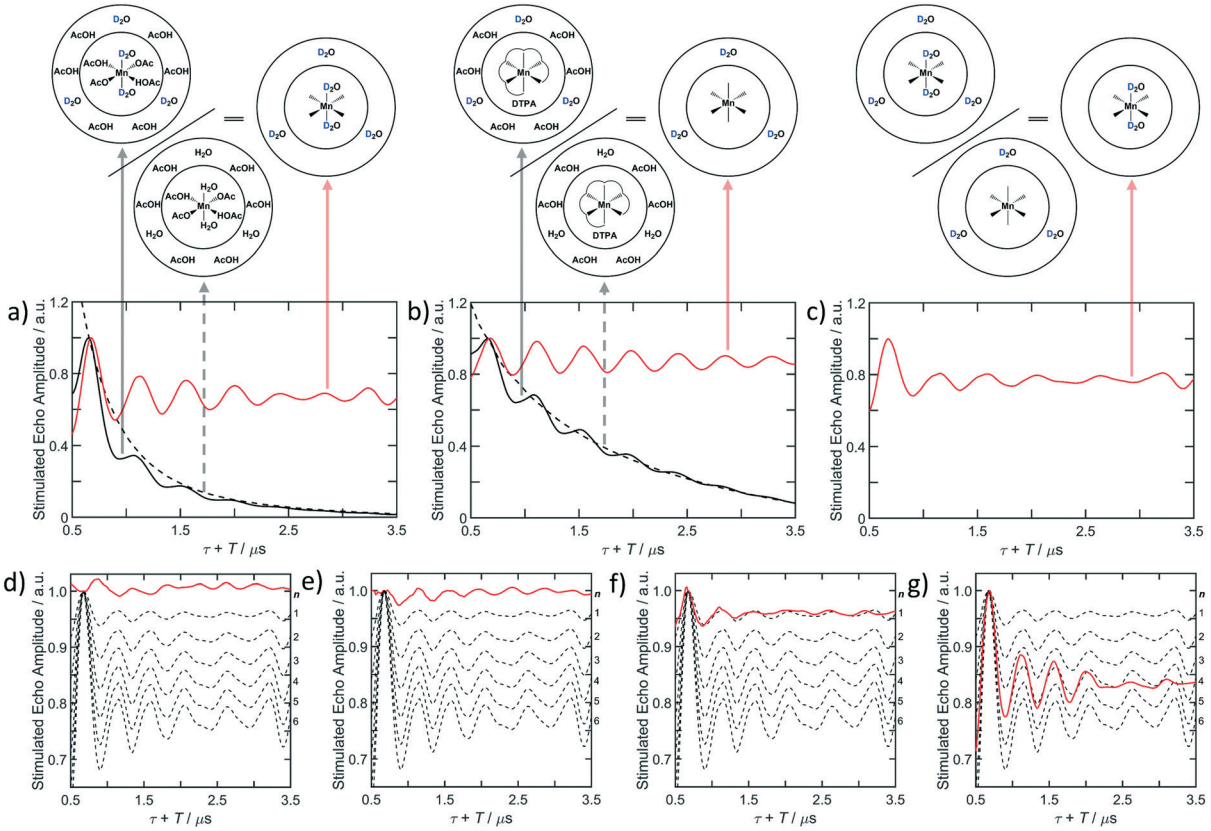

Fig. 3 Three-pulse ESEEM time domain data and corresponding ratios for $Mn(H_2O)_6^{2+}$. a) Raw data for $MnCl_2$ dissolved in D_2O (solid black line), H_2O (dashed line), and D/H ratio (solid red line). b) Corresponding traces for MnDTPA dissolved in D_2O (solid black line), H_2O (dashed line), and D/H ratio (solid red line). c) Trace revealing the isolated inner-sphere ^2H interactions, obtained as the ratio of the solid red traces in a) and b). Processed three pulse ESEEM data (solid red line) for the Mn^{2+} centre in H_2O/AcOH compositions of d) 3 wt%, e) 8 wt%, f) 13.7 wt%, and g) 20 wt% H_2O content. The scaled time traces for one to six inner sphere water ligands bound to $Mn(H_2O)_6^{2+}$ are shown in the dashed lines.

$Mn(H_2O)_6^{2+}$ reference system. The comparison between the modulation depths of the Mn/Br species and the reference sample, which has a known number of D_2O ligands and a comparable hyperfine to the analyte (see ESI† for further considerations on the choice of reference), provides a way of estimating the number of water molecules directly coordinated to the Mn^{2+} ion. For samples containing both 3 wt% and 8 wt% H_2O contents, the results are consistent with the presence of dehydrated Mn^{2+} centres (Fig. 3d and e). This is shown by the very shallow residual modulation depths observed after the double ratioing procedure, which are smaller than that which would correspond to one ligated water molecule. ESEEM evidence would suggest that in the low water content regime (*i.e.*, <8 wt% water in the solvent system), water does not tend to bind to the metal ions. The role of water appears to mostly increase the polarity of the solvent system by allowing increasingly more acetic acid to dissociate into acetate ions as the water content is increased. As acetate is a better ligand than acetic acid and bromide, an increased water content in this regime causes an increased displacement of ligated bromide ions (and to some extent non-dissociated acetic acid) at the advantage of acetate ions. This corroborates the changes observed in the UV-vis spectra (Fig. 2a) shown above. For water contents greater than 8 wt%, UV-vis spectroscopy on the Co^{2+} centre highlighted the absence of any cobalt bromide species. Although this UV-vis analysis is only possible with the Co^{2+} centre, the maximum broadening of the CW EPR linewidth of Mn^{2+} was observed up to *ca.* 8–10 wt% H_2O (Fig. 2b). In addition to EPR studies performed on Mn^{2+} in H_2O/AcOH at different compositions (see ESI†), this evidence collectively suggests a similar behaviour for manganese bromide species. Interestingly, in this high water content regime (*i.e.*, >13.7 wt% water in the solvent system), water seems to be present in the inner coordination sphere of Mn^{2+}. ESEEM data (Fig. 3f and g) indicates that at 13.7 wt% (34.6 mol%) and 20 wt% (45.4 mol%), an average of 1 and 4 water molecules respectively are directly bound per Mn^{2+} centre. At temperatures typical of the actual catalysis, these 1 to 4 water molecules per Mn centre measured in frozen solutions are likely to be ensemble averages where species with slightly higher or lower water coordination can also be present. Assuming octahedral geometry around the metal centre, and having excluded the presence of Br directly bonded to Mn^{2+}, the other possible ligands besides water must be acetate/acetic acid.

The combined evidence from CW EPR, ESEEM, UV-vis spectroscopies and static dielectric constant measurements,

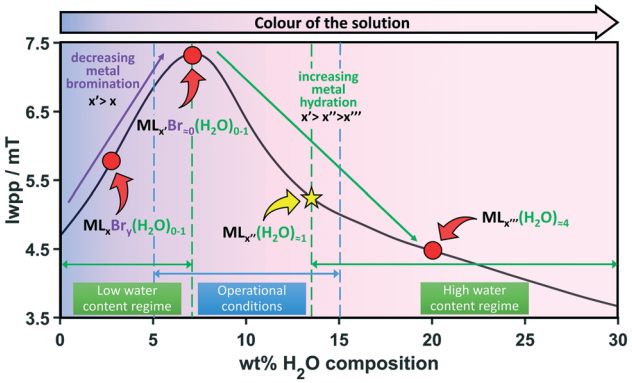

Fig. 4 Schematic diagram summarising the changing coordination environment of the metal centre (M) of the *para*-xylene oxidation catalyst as a function of solvent composition. L indicates either acetic acid or acetate ligands.

is of particular interest when considered within the context of the typical industrial conditions empirically adopted when oxidising *para*-xylene involving a solvent system containing 5 wt% to 15 wt% of water, and is summarised in Fig. 4. Interestingly, this range of H_2O compositions overlap with the transition from low to high water content regime highlighted earlier in our EPR analysis (Fig. 2). It is known for example that the increased reaction rates and low selectivity towards PTA are typically observed at very low water content.[6] Our results would suggest that this behaviour is mostly associated with the presence of dehydrated and de-acetated manganese and cobalt bromides. On the contrary, catalyst deactivation normally occurs at very high water concentrations.[7] According to our data, this can be attributed to the Mn^{2+} centres becoming too hydrated (*i.e.*, ESEEM revealed an average of 4 water molecules in the inner coordination sphere of Mn^{2+} at 20 wt%). The ideal conditions for optimum reaction rate and selectivity would appear to be associated with a low degree of metal ion hydration (at the advantage of acetate/acetic acid ligands), coupled to low levels of bromide ions in their inner coordination sphere.

Conclusions

The catalytic performance of the *para*-xylene oxidation catalyst system, including the reaction yield and selectively, is known to be inherently linked to the solvent composition, specifically the H_2O/AcOH ratio. However, the direct influence and correlation between these variable solvent compositions and the Co/Mn/Br catalyst structure are currently poorly understood. In this work, we have revealed how the coordination environment, as a function of the solvent composition, for this industrially important reaction can be characterised using advanced EPR methods and complimentary UV-vis measurements. The UV-vis analysis on the Co^{2+} component of the catalyst showed that reduced water content in the solvent (below 8 wt% H_2O) promotes Br coordination to Co^{2+}, forming a distribution of tetrahedral Co^{2+} species with 2 and 3 Br^- ligands at room temperature. Higher temperatures also promote the ligation of additional Br to the Co^{2+} centres for a fixed water composition. Changes to the CW EPR linewidth of the Mn^{2+} component of the catalyst showed a marked dependence on the H_2O/AcOH solvent composition, with a linewidth maximum observed at 8–10 wt% H_2O. This variation in linewidth was attributed to changes in the Mn^{2+} coordination environment, which in turn affects the chemical exchange-induced fluctuations in the ZFS on the EPR timescale (as manifested in the EPR linewidth). Water contents below 8 wt% produced narrow linewidths due to substitution of H_2O/AcOH ligands by Br, whereas above 8–10 wt%, the narrow linewidths were caused by increased H_2O coordination to the Mn^{2+} centres.

These findings from the CW EPR analysis were also corroborated by 3-pulse ESEEM measurements of the Mn^{2+} centre, enabling the number of coordinated H_2O molecules to Mn^{2+} to be determined (*i.e.*, a 'water counting' method). At 3 and 8 wt% H_2O, the Mn^{2+} centre is effectively dehydrated (n = 0 for H_2O coordination). The water thus serves to increase the solvent polarity, allowing more acetic acid to dissociate into acetate ions as the water content is increased. As acetate is a better ligand than acetic acid and bromide, the increased water content in this low wt% H_2O regime causes an increased displacement of ligated bromide ions (and to some extent non-dissociated acetic acid) at the expense of acetate ions. At the higher water compositions (*i.e.*, 13.7 and 20 wt% H_2O), Br is fully displaced due to the increased water coordination (an average of n = 1 and 4 for H_2O coordination per Mn^{2+} centre respectively), with the remaining ligands being acetic acid/acetate. Our ESEEM investigation is showing the level of water ligation per Mn centre. At the moment we cannot differentiate between monometallic and polymetallic species (the latter facilitated by acetate bridges). More investigation on this topic is needed, including an ESEEM protocol similar as the one adopted here but targeting acetic acid/acetate rather than water. Within the context of the industrial catalytic system, where the empirically accepted optimum H_2O/AcOH composition falls in the range of 5–15 wt% H_2O, the known increase in reaction rate and lower selectivity of the catalyst has in the past been attributed to lower water concentrations. The current results provide direct experimental evidence for the first time to support this interpretation; at low wt% H_2O, no H_2O coordination and higher Br coordination occurs to the metal centres in the 1/1/2 Co/Mn/Br catalysts, in the same range where best catalyst performance is reported, whereas the known catalyst deactivation in these reactions which occurs at >15 wt% H_2O, appears to result from increased H_2O coordination to the metal centres ($M(H_2O)_{n=1-4}$).

Conflicts of interest

There are no conflicts to declare.

Acknowledgements

Funding from Koch Technology Solutions Ltd and EPSRC (EP/L016443/1) is gratefully acknowledged.

Notes and references

1 Koch Technology Solutions - PTA, **https://www.kochtechsolutions.com/technologies/polyester-value-chain//**.
2 W. Partenheimer, *J. Mol. Catal.*, 1991, **67**, 35–46.
3 Y. Chen, J. L. Fulton and W. Partenheimer, *J. Am. Chem. Soc.*, 2005, **127**, 14085–14093.
4 W. Partenheimer, *Catal. Today*, 1995, **23**, 69–158.
5 W. Partenheimer, *Adv. Synth. Catal.*, 2004, **346**, 297–306.
6 V. A. Adamian and W. H. Gong, in *Liquid Phase Aerobic Oxidation Catalysis Industrial Applications and Academic Perspectives*, ed. S. S. Stahl and P. L. Alsters, WILEY-VCH, 1st edn, 2016, ch. 4, vol. 1, pp. 41–66.
7 R. A. F. Tomás, J. C. M. Bordado and J. F. P. Gomes, *Chem. Rev.*, 2013, **113**, 7421–7469.
8 P. Höfer, in *Electron Paramagnetic Resonance: A Practitioner's Toolkit*, ed. M. Brustolon and E. Giamello, Wiley, 2008, ch. 2, pp. 37–82.
9 S. S. Eaton and G. R. Eaton, in *Handbook of EPR Spectroscopy: Fundamentals and Methods*, ed. D. Goldfarb and S. Stoll, Wiley, 2018, ch. 9, pp. 175–192.
10 N. Bloembergen and L. O. Morgan, *J. Chem. Phys.*, 1961, **34**, 842–850.
11 N. Bloembergen, *J. Chem. Phys.*, 1957, **27**, 572–573.
12 K. E. Bett and J. B. Cappi, *Nature*, 1965, **207**, 620–621.
13 P. C. Kang, G. R. Eaton and S. S. Eaton, *Inorg. Chem.*, 1994, **33**, 3660–3665.
14 M. Idešicová, J. Titiš, J. Krzystek and R. Boča, *Inorg. Chem.*, 2013, **52**, 9409–9417.
15 J. W. P. Schmelzer, E. D. Zanotto and V. M. Fokin, *J. Chem. Phys.*, 2005, **122**, 74511.
16 M. W. Makinen, L. C. Kuo, M. B. Yim, G. B. Wells, J. M. Fukuyama and J. E. Kim, *J. Am. Chem. Soc.*, 1985, **107**, 5245–5255.
17 L. C. Kuo and M. W. Makinen, *J. Am. Chem. Soc.*, 1985, **107**, 5255–5261.
18 D. Piwowarska, P. Gnutek and C. Rudowicz, *Appl. Magn. Reson.*, 2019, **50**, 797–808.
19 M. H. Dean and G. Skirrow, *Trans. Faraday Soc.*, 1958, **54**, 849.
20 P. J. Proll, L. H. Sutcliffe and J. Walkley, *J. Phys. Chem.*, 1961, **65**, 455–460.
21 W. Partenheimer, J. L. Fulton, C. M. Sorensen, V.-T. Pham and Y. Chen, *J. Mol. Catal. A: Chem.*, 2014, **387**, 130–137.
22 K. Sawada and M. Tanaka, *J. Inorg. Nucl. Chem.*, 1977, **39**, 339–344.
23 A. N. Campbell and J. M. T. M. Gieskes, *Can. J. Chem.*, 1964, **42**, 1379–1387.
24 C. P. Smyth and H. E. Rogers, *J. Am. Chem. Soc.*, 1930, **52**, 1824–1830.
25 C. G. Hoogstraten and R. D. Britt, *RNA*, 2002, **8**, 252–260.